Triple Differential Cross Sections for the Double Photoionization of H_2

J. Colgan,[1] M. S. Pindzola,[2] and F. Robicheaux[2]
[1]*Theoretical Division, Los Alamos National Laboratory, Los Alamos, New Mexico 87545, USA*
[2]*Department of Physics, Auburn University, Auburn, Alabama 36849, USA*
(Received 11 December 2006; published 9 April 2007)

Triple differential cross sections arising from the break up of the H_2 molecule by a single photon are presented. The time-dependent close-coupling technique is used to calculate differential cross sections for various geometries. Excellent agreement is found between current work and recent exterior complex-scaling calculations, confirming, for the first time, the absolute magnitude of the triple differential cross sections. Our calculations also compare favorably with recent synchrotron light source measurements.

DOI: 10.1103/PhysRevLett.98.153001 PACS numbers: 33.80.Eh

The differential cross sections arising from the removal of both electrons from the H_2 molecule by a single photon has long been an outstanding problem in collision physics. This quantity is the most sensitive test of the correlation between the outgoing continuum electrons moving in the resulting Coulomb molecular field. This case is an example of a Coulomb four-body problem, although it is simplified somewhat since the electrons leave the molecule well before the nuclei begin to explode apart, so that the fixed-nuclei approximation is well founded. In contrast to the simpler Coulomb three-body problem found in the double photoionization (DPI) of helium, where theory and experiment agree for practically all measurable parameters [1–5], H_2 has received much less attention theoretically, due to the increased complexity of following two electrons moving in a Coulomb field formed by an ionized molecule. Important progress has been made by Feagin [6] and Walter and Briggs [7], who described selection rules for the molecular photoionization process. Although the problem has been systematically studied by synchrotron light source experiments [8–13], it is only very recently that theory has been able to tackle the problem in a rigorous manner [14–17].

In this Letter we present, for the first time, triple differential cross sections for the DPI of H_2 using the time-dependent close-coupling approach. Our calculated cross sections are in excellent agreement in both magnitude and shape with very recent theoretical calculations made using the exterior complex-scaling (ECS) technique [16,17], and, when averaged over the angular uncertainties of recent experimental measurements [10], are also in very good agreement with these measurements. The excellent agreement that now exists between two completely independent theoretical techniques brings the double photoionization of H_2 onto the same level as the double photoionization of He, a three-body Coulomb problem, where excellent agreement has existed for some time between several theoretical methods and experiment.

Our previous work on this subject using the time-dependent close-coupling method (TDCC) [14] allowed the calculation of only the total double photoionization cross section. Here we show how our method can be extended to calculate differential cross sections. Atomic units are used throughout.

In the weak-field perturbative limit, the photoionization of the H_2 molecule may be found by solving the time-dependent Schrödinger equation [18]:

$$i\frac{\partial\psi(\vec{r}_1,\vec{r}_2,t)}{\partial t} = H\psi(\vec{r}_1,\vec{r}_2,t) + V\psi_0(\vec{r}_1,\vec{r}_2)e^{-iE_0t}, \quad (1)$$

where H is the molecular Hamiltonian, V is the time-dependent radiation field Hamiltonian, and ψ_0 and E_0 are the exact eigenfunction and eigenenergy of the molecular ground state. Because of the reduced symmetry of the molecular case, the time-dependent wave function for a given MS symmetry is expanded in products of rotation functions:

$$\psi(\vec{r}_1,\vec{r}_2,t) = \sum_{m_1,m_2}\frac{P^M_{m_1m_2}(r_1,\theta_1,r_2,\theta_2,t)}{r_1r_2\sqrt{\sin\theta_1}\sqrt{\sin\theta_2}}\Phi_{m_1}(\phi_1)\Phi_{m_2}(\phi_2), \quad (2)$$

where $\Phi_m(\phi) = e^{im\phi}/\sqrt{2\pi}$ and $M = m_1 + m_2$ is the projection of total electronic angular momentum onto the z axis. For ionization of the ground state of H_2 the total spin angular momentum S is zero. Upon substitution of Eq. (2) into Eq. (1) and application of the variational principle, the time-dependent close-coupled partial differential equations are given by

$$i\frac{\partial P^M_{m_1m_2}(r_1,\theta_1,r_2,\theta_2,t)}{\partial t} = T_{m_1,m_2}(r_1,\theta_1,r_2,\theta_2)P^M_{m_1m_2}(r_1,\theta_1,r_2,\theta_2,t) + \sum_{m_1'm_2'}V^M_{m_1m_2,m_1'm_2'}(r_1,\theta_1,r_2,\theta_2)P^M_{m_1'm_2'}(r_1,\theta_1,r_2,\theta_2,t)$$
$$+ \sum_{m_1'',m_2''}W^{MM_0}_{m_1m_2,m_1''m_2''}(r_1,\theta_1,r_2,\theta_2,t)\bar{P}^{M_0}_{m_1''m_2''}(r_1,\theta_1,r_2,\theta_2)e^{-iE_0t}, \quad (3)$$

where expressions for the various kinetic energy, one-electron potential, and two-electron potential terms may be found in [14], and $\bar{P}^{M_0}_{m_1 m_2}$ is the reduced wave function for ψ_0. The exact lattice eigenfunction for the H_2 ground state is obtained by relaxation of the Schrödinger equation in imaginary time ($\tau = it$):

$$-\frac{\partial \psi_0(\vec{r}_1, \vec{r}_2, \tau)}{\partial \tau} = H\psi_0(\vec{r}_1, \vec{r}_2, \tau). \tag{4}$$

The wave function ψ_0 is expanded in products of rotation functions and substituted into Eq. (4), yielding a set of close-coupled partial differential equations in space and imaginary time.

We solve the time-dependent close-coupling equations using lattice techniques to obtain a discrete representation of the reduced wave functions and all operators on a four-dimensional radial and angular grid. A $384 \times 384 \times 32 \times 32$ point lattice is employed with a uniform mesh spacing of 0.1 a.u. in both r_1 and r_2 and a mesh spacing of $0.031\,25\pi$ in both θ_1 and θ_2. Seven coupled channels were employed in both the relaxation to the initial $^1\Sigma_g$ state, and in the real time propagation to the final $M = 0$ symmetry. Eight coupled channels were employed in the real time propagation to the final $M = \pm 1$ symmetry. The boundary condition at $t = 0$ for the reduced wave function is simply $P^M_{m_1 m_2}(r_1, \theta_1, r_2, \theta_2, t = 0) = 0$.

The total cross section for double photoionization for a given M symmetry can be written as

$$\sigma_{\text{dion}} = \frac{\omega}{I}\frac{\partial \mathcal{P}_{\text{dion}}}{\partial t}, \tag{5}$$

where the double photoionization probability, $\mathcal{P}_{\text{dion}}$, has been defined in [14] in terms of summing projections onto the remaining bound states of the molecular ion. The double photoionization probability for a particular M value can also be given by

$$\mathcal{P}_{\text{dion}} = \sum_{l_1 l_2}\sum_{m_1 m_2}\int dk_1 \int dk_2 P^M_{l_1 m_1 l_2 m_2}(k_1, k_2, T), \tag{6}$$

where the momentum-space wave functions, $P^M_{l_1 m_1 l_2 m_2}(k_1, k_2, T)$, are defined as

$$P^M_{l_1 m_1 l_2 m_2}(k_1, k_2, T) = \int_0^\infty dr_1 \int_0^\pi d\theta_1 \int_0^\infty dr_2 \int_0^\pi d\theta_2 P^M_{m_1 m_2}(r_1, \theta_1, r_2, \theta_2, T) P^*_{k_1 l_1 m_1}(r_1, \theta_1) P^*_{k_2 l_2 m_2}(r_2, \theta_2). \tag{7}$$

We note that the phase of the complex distorted waves used in this projection is contained within the S matrix boundary conditions used in their generation. In our calculations all orbital angular momenta up to $l = 7$ were retained in the sum in Eq. (6). The single differential cross section for double photoionization of H_2 can be written as [19]

$$\frac{d\sigma}{d\alpha} = \frac{\omega}{I}\frac{\partial}{\partial t}\int dk_1 \int dk_2 \delta\left(\tan\alpha - \frac{k_2}{k_1}\right) \times \sum_{l_1 m_1, l_2 m_2} |P^M_{l_1 m_1 l_2 m_2}(k_1, k_2, T)|^2, \tag{8}$$

with the single differential cross section in ejected- energy given by

$$\frac{d\sigma}{dE_1} = \frac{1}{E_1 E_2}\frac{d\sigma}{d\alpha}, \tag{9}$$

where E_1 is the energy of one of the ejected electrons and α is the hyperspherical angle between the two outgoing electron momenta. This single differential cross section has been shown to have a very similar shape to the He case [19], and integrates over ejected energy to recover the total integral cross section. The single differential cross sections for each M (where $M = 0$ corresponds to a transition to a final Σ state, and $M = \pm 1$ corresponds to a transition to a final Π state) can also be used to extract the ion asymmetry (β) parameter. At equal energy sharing we find an asymmetry parameter of -0.802, which is within 2% of the value quoted by Vanroose *et al.* [17], and in good agreement with the experimental measurement of -0.73 ± 0.1 [10].

We can now express the triple differential cross section for double photoionization of H_2 for the case where the polarization axis is oriented at an arbitrary solid angle (θ_N, ϕ_N) to the molecular internuclear distance as

$$\frac{d^3\sigma}{d\alpha d\Omega_1 d\Omega_2} = \frac{\omega}{I}\frac{\partial}{\partial t}\int dk_1 \int dk_2 \delta\left(\tan\alpha - \frac{k_2}{k_1}\right)|\mathcal{M}|^2, \tag{10}$$

where Ω_1 and Ω_2 are the solid angles in which the outgoing electrons are ejected [with $\Omega \equiv (\theta, \phi)$]. The amplitude $\mathcal{M}$ is given by

$$\begin{aligned}\mathcal{M} = \sum_{l_1 l_2}\sum_{m_1 m_2}(-i)^{l_1+l_2} e^{i(\sigma_{l_1}+\sigma_{l_2})}\Big\{&\cos\theta_N P^{M=0}_{l_1 m_1 l_2 m_2}(k_1, k_2, T) Y_{l_1 m_1}(\hat{k}_1) Y_{l_2 m_2}(\hat{k}_2)\delta_{m_1+m_2,0} \\ &+ \sin\theta_N\left[\frac{\cos\phi_N - i\sin\phi_N}{\sqrt{2}}\right] P^{M=+1}_{l_1 m_1 l_2 m_2}(k_1, k_2, T) Y_{l_1 m_1}(\hat{k}_1) Y_{l_2 m_2}(\hat{k}_2)\delta_{m_1+m_2,1} \\ &+ \sin\theta_N\left[\frac{\cos\phi_N + i\sin\phi_N}{\sqrt{2}}\right] P^{M=-1}_{l_1 m_1 l_2 m_2}(k_1, k_2, T) Y_{l_1 m_1}(\hat{k}_1) Y_{l_2 m_2}(\hat{k}_2)\delta_{m_1+m_2,-1}\Big\},\end{aligned} \tag{11}$$

where in this equation σ_l is the Coulomb phase and $Y_{lm}(\hat{k})$ represents a spherical harmonic.

In Figs. 1–3 we present the triple differential cross sections for H_2 for an excess energy of 25 eV with the energy shared equally among the outgoing electrons. In the planar plots we compare with ECS calculations [16,17] and in the polar plots (insets) with experimental measurements [10]. In comparing with the measurements we have averaged over the experimental uncertainties in the molecular orientation angles and in the ejected electron angles (which were typically $\theta_N = \pm 20°$; $\phi_N = \pm 90°$; $\theta_1 = \pm 15°$; $\phi_1 = \pm 20°$) [20]. Also, the measurements were reported as absolute with units of mb/(eV^2 sr^3), since the measurements are differential in outgoing energy of both electrons and in the solid angles between the polarization and molecular axes. Since our calculations are for fixed internuclear separation (which implies a cross section differential in only one of the outgoing electron energies), and for fixed molecular orientations, we compute a triple differential cross section, in units of b/(eV sr^2). Thus, to compare with the measurements, we renormalize our calculations to the experimental data. The same normalization has been used for all the calculations in the insets of Figs. 1–3. We do emphasize, however, that the TDCC triple differential cross sections presented in the Cartesian plots are absolute and not normalized in any way.

In Figs. 1 and 2 the first electron is detected at an angle of 90° and 0°, respectively, and coplanar with the polarization direction, which always lies along the z axis. The agreement between the new TDCC calculations and the ECS calculations [17] is excellent for all orientations of the molecule and for both the shape and magnitude of the differential cross sections. Similar good agreement is found in Fig. 3, where in these cases the first electron is detected out of the plane, and the molecule is oriented in three different directions: (a) out of the plane; (b) perpendicular to the z axis, but coplanar; and (c) along the z axis. The nodes in Figs. 1 and 2 at $\theta_2 = 270°$ and $\theta_2 = 180°$, respectively (corresponding to $\theta_{12} = 180°$), also confirm the selection rules discussed by [7]. The agreement between these two independent theoretical methods for all cases is a very strong indication that the correct physics is described in both theories. This is remarkable considering the completely different approaches taken in both methods. The ECS method is a time-independent approach, which obviates the need for asymptotic boundary conditions for the two outgoing electrons by rotating the two-electron wave function into the complex plane. The TDCC approach solves the time-dependent Schrödinger equation numerically in real time and so avoids the need for boundary conditions. Both techniques use a fully correlated initial ground state of the H_2 system as a starting point, and fully treat the correlation between the outgoing electrons.

The agreement between the TDCC results and the measurements is also very good. In all cases the shape predicted by the TDCC results, when averaged over the experimental uncertainties, is in good agreement with the measurement. We do note, however, some discrepancy in the magnitudes of the triple differential cross section observed by experiment and predicted by theory. In particular, differences are found in Fig. 1(d), and for all cases in Fig. 2, as was also noted by Vanroose *et al.* [17]. For these cases, the calculations are consistently larger than the measurements. This may be related to the larger β parameter predicted by our calculations as compared to the measured parameter [10], which may partly explain why the

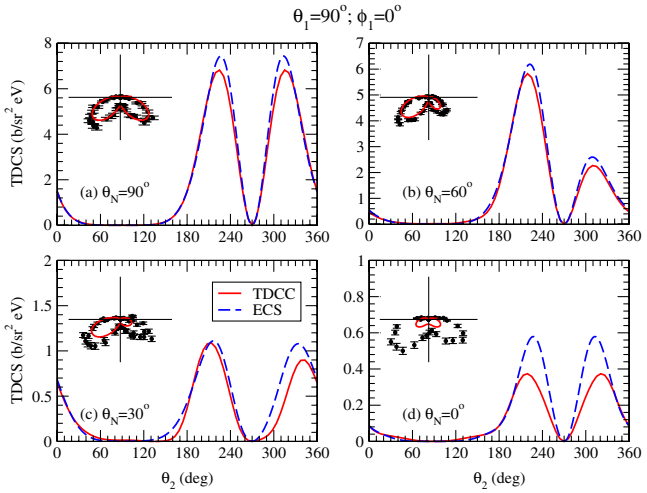

FIG. 1 (color online). Triple differential cross sections for H_2 for excess photon energies of 25 eV, with equal energy sharing between the electrons, for various molecular orientations, as indicated, and for $\theta_1 = 90°$, $\phi = 0°$. We compare the TDCC calculations (solid red lines) with ECS calculations (dashed blue lines) [15], and with experimental measurements (solid black circles) [8]. The units of the inset polar plots are mb/(eV^2 sr^3), where the radii of the thin black lines equal magnitudes of 120, 120, 50, and 30 mb/(eV^2 sr^3), for (a)–(d), respectively.

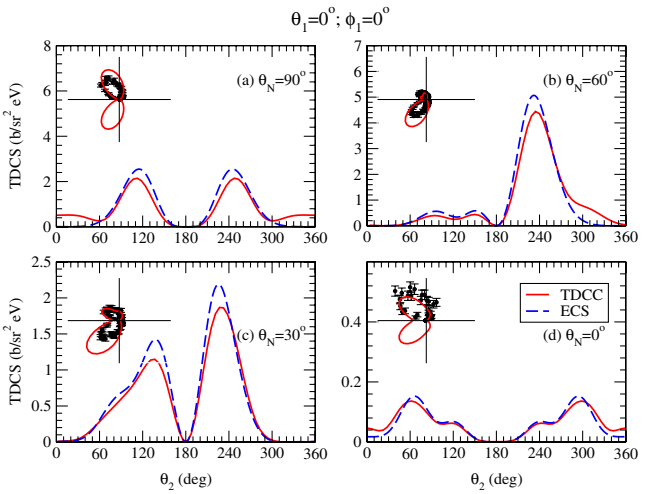

FIG. 2 (color online). As in Fig. 1, for the case where $\theta_1 = 0°$, $\phi_1 = 0°$. The units of the inset polar plots are mb/(eV^2 sr^3), where the radii of the thin black lines equal magnitudes of 50, 80, 40, and 15 mb/(eV^2 sr^3), for (a)–(d), respectively.

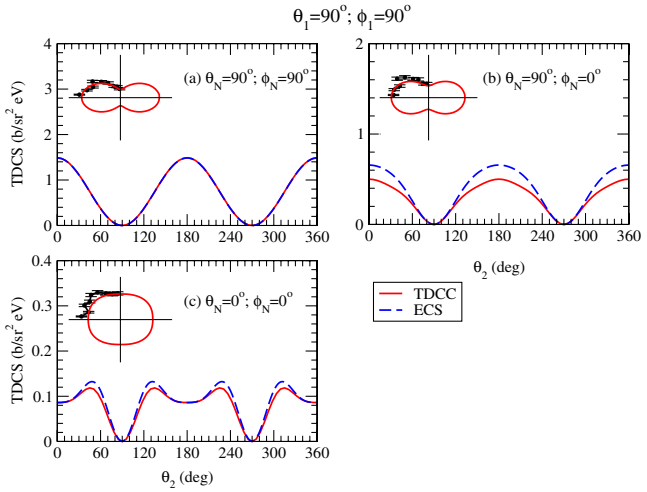

FIG. 3 (color online). As in Fig. 1, for the case where $\theta_1 = 90°$ and $\phi_1 = 90°$; see text for details. The units of the inset polar plots are mb/(eV^2 sr^3), where the radii of the thin black lines equal magnitudes of 30, 20, and 10 mb/(eV^2 sr^3), for (a)–(c), respectively.

calculations are larger in Fig. 2(a). It is also interesting that, in general, very good agreement is obtained for the cross section magnitude between theory and experiment for almost all cases of Fig. 1, but not for Fig. 2. More detailed comparison with experiment is needed to resolve such issues.

We also note that the uncertainties in the measurements, particularly in the angle of orientation between the polarization and internuclear axes, masks somewhat the nature of the differential cross section. This is most evident for Figs. 1(d) and 2(d), where the calculations are made at exactly $\theta_N = 0°$, i.e., the pure Σ transition case. Because of the much larger magnitude of the $M = \pm 1$ (Π) transitions, the uncertainties in the measurements of θ_N, which range from $\pm 20°$ to $\pm 30°$, introduce "contaminating" cross sections into the measurements in Figs. 1(d) and 2(d). As can be seen in comparing the shapes of the theoretical calculations for the pure Σ case with the measurements, this results in a quite different triple differential cross section in these cases. For example, in Fig. 2(d), the forward lobe observed at $\theta_2 = 60°$ in the calculations appears at $\theta_2 = 135°$ in the measurements (and averaged calculations) because of the influence of the dominating Π transition. For similar reasons, the uncertainty in the measurements for large θ_N make very little difference to the shape of the cross sections [e.g., Figs. 1(a) and 2(a)] since the magnitude of the Σ transition is much smaller than the Π transition and so has little effect on the shape of the differential cross section.

In summary, we have demonstrated that the time-dependent close-coupling method is suitable for computing accurate triple differential cross sections for the double photoionization of H_2. The close agreement found between our calculations and the results from the ECS method [17] provide a benchmark for the magnitudes and shapes of these triple differential cross sections. When suitably averaged over experimental uncertainties, our calculations are also in good agreement with recent measurements [10]. In future work we intend to use our method to explore how the triple differential cross sections (and thus the role of final-state electron correlations) change as a function of internuclear separation, as well as how these quantities develop in time. Interesting molecular effects may exist which appear to change the electron distributions as the molecule lengthens [8]. It may also be possible to investigate which geometries reach their final cross sections quickly in time, and which ones take longer in time to converge. This ability is a strength of our time-dependent method and should allow us to examine more fully the role of final-state correlations.

We thank M. Gisselbrecht and D. Horner for providing us with their data in numerical form, and T. Reddish and A. Huetz for useful discussions. A portion of this work was performed under the auspices of the U.S. DOE through Los Alamos National Laboratory and through a grant to Auburn University. Computational work was carried out at NERSC in Oakland, CA, the NCCS in Oak Ridge, TN, through the Los Alamos National Laboratory Institutional Computing Resources and the MSCF at Pacific Northwest National Laboratory.

[1] A. S. Kheifets and I. Bray, J. Phys. B **31**, L447 (1998).
[2] L. Malegat *et al.*, Phys. Rev. Lett. **85**, 4450 (2000).
[3] J. Colgan *et al.*, J. Phys. B **34**, L457 (2001).
[4] C. W. McCurdy *et al.*, Phys. Rev. A **69**, 032707 (2004).
[5] H. Brauning *et al.*, J. Phys. B **31**, 5149 (1998).
[6] J. M. Feagin, J. Phys. B **31**, L729 (1998).
[7] M. Walter and J. Briggs, J. Phys. B **32**, 2487 (1999).
[8] T. Weber *et al.*, Phys. Rev. Lett. **92**, 163001 (2004); Nature (London) **431**, 437 (2004).
[9] R. Dorner *et al.*, Phys. Rev. Lett. **81**, 5776 (1998).
[10] M. Gisselbrecht *et al.*, Phys. Rev. Lett. **96**, 153002 (2006).
[11] S. A. Collins *et al.*, Phys. Rev. A **64**, 062706 (2001).
[12] P. Bolognesi *et al.*, J. Phys. B **36**, L241 (2003).
[13] D. P. Seccombe *et al.*, J. Phys. B **35**, 3767 (2002).
[14] J. Colgan *et al.*, J. Phys. B **37**, L377 (2004).
[15] W. Vanroose *et al.*, Phys. Rev. A **70**, 050703 (2004).
[16] W. Vanroose *et al.*, Science **310**, 1787 (2005).
[17] W. Vanroose *et al.*, Phys. Rev. A **74**, 052702 (2006).
[18] M. S. Pindzola and F. Robicheaux, Phys. Rev. A **57**, 318 (1998).
[19] J. Colgan *et al.*, in *Ionization, Correlation, and Polarization in Atomic Collisions*, edited by A. Lahmam-Bennani and B. Lohmann, AIP Conf. Proc. No. 811 (AIP New York, 2006), p. 48.
[20] T. Reddish and A. Huetz (private communication).